

Characterization and Modeling of Native MOSFETs Down to 4.2 K

Yuanke Zhang, Tengting Lu, Wenjie Wang, Yujing Zhang, Jun Xu, Chao Luo, Guoping Guo

Abstract—The extremely low threshold voltage (V_{TH}) of native MOSFETs ($V_{TH} \approx 0$ V @ 300 K) is conducive to the design of cryogenic circuits. Previous research on cryogenic MOSFETs mainly focused on the standard threshold voltage (SVT) and low threshold voltage (LVT) MOSFETs. In this paper, we characterize native MOSFETs within the temperature range from 300 K to 4.2 K. The cryogenic V_{TH} increases up to ~ 0.25 V ($W/L = 10 \mu\text{m}/10 \mu\text{m}$) and the improved sub-threshold swing (SS) ≈ 14.30 mV/dec @ 4.2 K. The off-state current (I_{OFF}) and the gate-induced drain leakage (GIDL) effect are ameliorated greatly. The step-up effect caused by the substrate charge and the transconductance peak effect caused by the energy quantization in different sub-bands are also discussed. Based on the EKV model, we modified the mobility calculation equations and proposed a compact model of large size native MOSFETs suitable for the range of 300 K to 4.2 K. The mobility-related parameters are extracted via a machine learning approach and the temperature dependences of the scattering mechanisms are analyzed. This work is beneficial to both the research on cryogenic MOSFETs modeling and the design of cryogenic CMOS circuits for quantum chips.

Index Terms—Cryogenic, native MOSFETs, characterization, modeling, cryogenic effects, mobility, scattering mechanism.

I. INTRODUCTION

CRYOGENIC CMOS (cryo-CMOS) technology has been studied widely in recent years and plays an important role in the readout and control circuits used for quantum chips [1] [2]. Cryogenic operation of CMOS circuits improves both the scalability and the system integration of quantum chips. Meanwhile, the quantum effects of cryogenic MOSFETs (e.g., Coulomb blocking) enable cryo-CMOS to build not only classical circuits but also quantum circuits [3]. However, cryo-CMOS technology still faces several challenges, including power limitations and cryogenic MOSFETs modeling. Because of the huge temperature gap and low-temperature effects involved, most of the classic models (e.g., BSIM3v3 [4], EKV2.6 [5]) are only suitable around room temperature (RT). Therefore, the research and modeling of cryogenic MOSFETs are necessary.

To date, characterization of MOSFETs technology in the range of $0.35 \mu\text{m}$ to 14 nm from 77 K to 50 mK has been widely reported [3], [6]–[10]. Most of these studies have

focused on standard threshold voltage (SVT) and low threshold voltage (LVT) MOSFETs, but few have characterized native MOSFETs ($V_{TH} \approx 0$ V @ 300 K), which can be used in high-speed and low operating voltage circuits. Because of the increase of substrate Fermi potential at cryogenic temperature, the high threshold voltages of cryogenic MOSFETs increase the design difficulty. Native MOSFETs represent a good choice ($V_{TH} < 0.3$ V @ 4.2 K). In addition, the kink effect [9] is alleviated in native MOSFETs because of their low substrate doping concentration (N_a) and low body effect parameter ($\gamma = \sqrt{2q\epsilon_{si}N_a}/C_{OX}$, C_{OX} is the gate oxide capacitance per unit area), thus simplifying the device modeling process.

In this paper, the low-temperature characteristics of native MOSFETs at temperatures ranging from 300 K to 4.2 K are presented, with particular focus on the step-up effect and the transconductance peak effect. In addition, the current drop (i.e., negative transconductance) behavior in the linear region transfer characteristics is the most noteworthy. By modifying the mobility equations of the EKV2.6 model, the mobility is calculated using scattering mechanisms, i.e., Coulomb scattering, surface roughness scattering, and phonon scattering, and the current drop behavior is reproduced well. Furthermore, the mobility-related parameters are extracted using a machine learning approach, and the temperature dependences of the scattering mechanisms are analyzed. Unlike the standard EKV2.6 model with its minimum applicable temperature of 230 K, the compact model of the large size native MOSFETs proposed in this paper is suitable for an extended temperature range from 300 K down to 4.2 K.

II. CRYOGENIC MEASUREMENT SETUP

The devices under test (DUT) in this paper were manufactured in a commercial SMIC $0.18 \mu\text{m}$ bulk MOSFETs process with 1.8 V nominal voltage. DUT were n-type native MOSFETs with $W/L = 10 \mu\text{m}/10 \mu\text{m}$ and $10 \mu\text{m}/1 \mu\text{m}$. We also characterized some SVT and LVT MOSFETs as the comparison. DC characteristics were performed by a Keysight B1500A semiconductor device analyzer, and the 4-wire method was taken to remove the influence of wire resistance. Liquid nitrogen/helium dewar was used to cool DUT from 300 K to 77 K/4.2 K. Transfer characteristics in linear/saturation regions ($I_{DS}-V_{GS}$, $V_{DS} = 50 \text{ mV}/1.8 \text{ V}$) and output characteristics ($I_{DS}-V_{DS}$, $V_{GS} = 0 \text{ V} \rightarrow 1.8 \text{ V}$, step = 0.3 V) were measured. The electrical properties of DUT were extracted: V_{TH} (using maximum transconductance method [3]), the drain saturation current (I_{DSAT} , $V_{DS} = V_{GS} = 1.8 \text{ V}$), the OFF-state drain

This work was supported by the National Natural Science Foundation of China (Grants No. 12034018). (Corresponding author: Chao Luo, e-mail: lc0121@ustc.edu.cn)

The authors are with Key Laboratory of Quantum Information, University of Science and Technology of China, Hefei, Anhui 230026, China.

leakage current (I_{OFF} , $V_{DS} = 1.8$ V and $V_{GS} = 0$ V), and the drain induced barrier lowering (DIBL) effect which is defined as $[V_{GS}(I_{DS} = 5 \times 10^{-7} \text{ A}, V_{DS} = 50 \text{ mV}) - V_{GS}(I_{DS} = 5 \times 10^{-7} \text{ A}, V_{DS} = 1.8 \text{ V})]/1.75 \text{ V}$.

III. CHARACTERIZATION

A. Cryogenic Measurement

Cryogenic operation can greatly improve MOSFETs performance. As shown in Fig. 1(a), we extracted V_{TH} , subthreshold swing (SS), I_{DSAT} , and I_{OFF} from the transfer characteristics at 300 K and 4.2 K, and listed them in Table I. At low temperatures, the intrinsic carrier concentration decreases and the Fermi energy level of the p-type substrate moves closer to the valence band, thus resulting in a significant increase of the Fermi potential. Therefore, V_{TH} increases to ~ 0.25 V. SS improves significantly, but is still much higher than the theoretical limit ($\ln(10)K_B T/q$, $\sim 0.83 \text{ mV/dec}$ @ 4.2 K); this can be attributed to the effect of the interface traps close to the band edges [8]. Additionally, the reduced I_{OFF} and improved I_{DSAT} strongly optimize the device ON/OFF ratio. The DIBL effect and the gate-induced drain leakage (GIDL) effect are also observed, as shown in Fig. 1(a). The reduced ionization rate causes the source/drain p-n⁺ junction depletion to broaden, thus reducing the effective channel length and aggravating the DIBL effect. The GIDL effect can be explained using the band-to-band tunneling (BTBT) process. At cryogenic temperatures, the larger bandgap elongates the tunneling distance, which then weakens the BTBT effect and reduces the leakage current in the negative V_{GS} region [11].

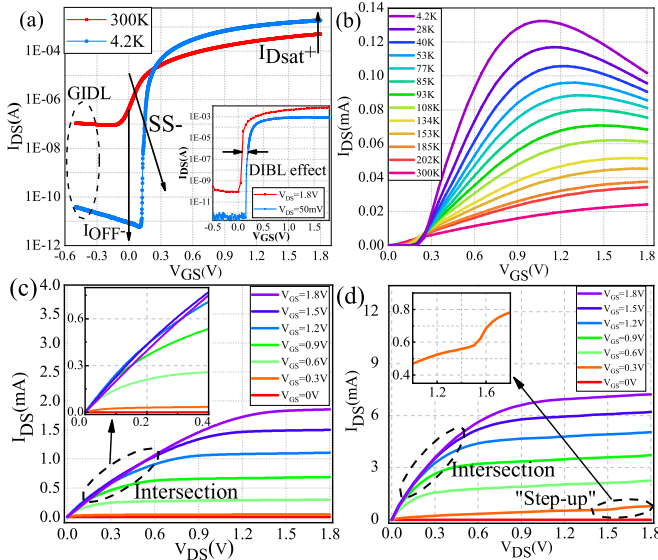


Fig. 1. DC Characteristics of native MOSFETs. (a) Comparison of the transfer characteristics in the saturation regions ($V_{DS} = 1.8$ V, $W/L = 10 \mu\text{m}/10 \mu\text{m}$) at 300 K and 4.2 K, respectively. Inset: transfer characteristics in the linear region and the saturation region ($V_{DS} = 50 \text{ mV}/1.8 \text{ V}$, $W/L = 10 \mu\text{m}/1 \mu\text{m}$) at 4.2 K. (b) Transfer characteristics in the linear region at various temperatures. (c) Output characteristics with $W/L = 10 \mu\text{m}/10 \mu\text{m}$ at 4.2 K. Inset: the enlarged view of the part circled by the dotted line (the intersection of output characteristics curves). (d) Output characteristics with $W/L = 10 \mu\text{m}/1 \mu\text{m}$ at 4.2 K. Inset: the enlarged view of the part circled by the dotted line (the step-up effect).

TABLE I
DC CHARACTERISTICS OF NATIVE NMOSFETS ($W/L = 10 \mu\text{m}/10 \mu\text{m}$) AT 300 K AND 4.2 K

Temperature	300 K	4.2 K
$V_{TH}(\text{mV})$	38.05	257.07
$SS(\text{mV/dec})$	86.25	14.30
$I_{DSAT}(\text{mA})$	0.511	1.852
$I_{OFF}(\text{A})$	4.39×10^{-7}	8.70×10^{-12}
I_{DSAT}/I_{OFF}	1.16×10^3	2.13×10^8
$DIBL(\text{mV/V})$ ($W/L = 10 \mu\text{m}/1 \mu\text{m}$)	35.429	80.571

Fig. 1(b) shows the linear region transfer characteristics from 300 K to 4.2 K. It should be noted that, with decreasing temperature, the curves show more pronounced current drop (i.e., negative transconductance) behaviors. This is caused by the change of the mobility behavior: at low temperatures, when V_{GS} increases, the increase of the number of carriers cannot compensate for the reduction of carrier mobility, thus causing I_{DS} to decrease. Fig. 1(c) and (d) show the output characteristics of native MOSFETs ($W/L = 10 \mu\text{m}/10 \mu\text{m}$ and $10 \mu\text{m}/1 \mu\text{m}$). Intersection of these curves can be observed in both figures. This phenomenon corresponds to the linear region current drop behavior that was described above: different V_{GS} may results in the same I_{DS} under the same V_{DS} . This phenomenon is described and discussed in detail in Section III. In addition, in Fig. 1(d), a step-up effect of a sudden I_{DS} increase is observed. To explore the physical mechanism behind this effect, we performed measurements with different delay times [10] at specific temperatures, with results as shown in Fig. 2.

B. Step-Up Effect

We applied delay times ranging from 1 ms to 10 s and performed both forward scans [Figs. 2(a)-(c)] and backward scans [Figs. 2(d)-(f)]. The splitting and the step-up behaviors of I_{DS} curves were observed under different delay times. Two mechanisms are involved in the above phenomena: the accumulation of substrate holes due to impact ionization and the dissipation of these holes via substrate/source parasitic capacitance, and both mechanisms are time-dependent. At low temperatures, the holes generated by impact ionization flow towards and accumulate in the freeze-out substrate, thus raising the substrate potential; this leads to a reduction of V_{TH} and thus a rise of I_{DS} , which is similar to the kink effect that occurs in SVT MOSFETs [9]. Additionally, the accumulated holes in the substrate can also be transferred to the source via the substrate/source parasitic capacitance, thus reducing the substrate potential.

In the lower V_{DS} range, e.g., region A in Fig. 2(a) and (b), a higher delay time results in a reduced I_{DS} . This is because carriers impact ionization produces fewer holes at lower V_{DS} . A longer delay time results in more complete hole dissipation in the substrate, i.e., lower substrate potential and thus smaller I_{DS} .

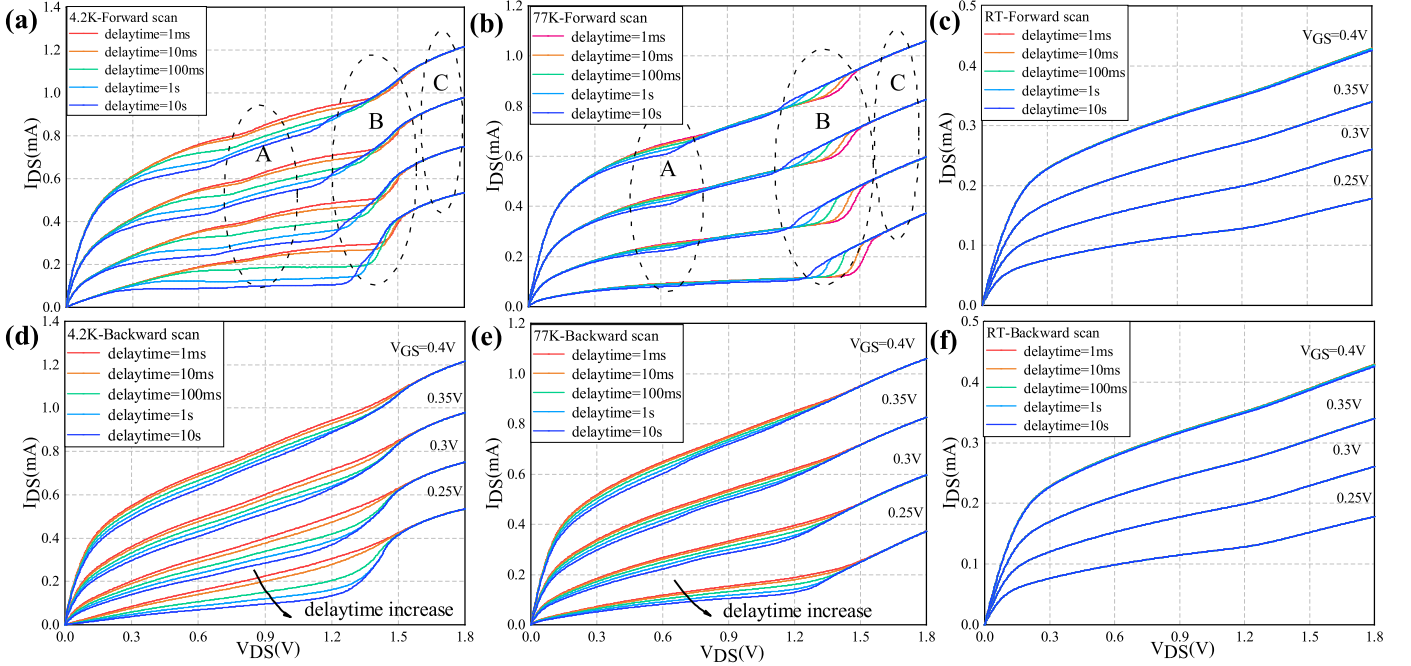


Fig. 2. Forward scans (a-c) and backward scans (d-f) of I-V characteristics for the native MOSFETs with $W/L = 10 \mu\text{m}/1 \mu\text{m}$ at different temperatures. (a,d) At 4.2 K. (b,e) At 77 K. (c,f) At RT. $V_{GS} = 0.25 \text{ V}/0.3 \text{ V}/0.35 \text{ V}/0.4 \text{ V}$.

In the regions where I_{DS} rise occurs, i.e., region B in Fig. 2(a) and (b), because of the higher V_{DS} , the number of holes generated by impact ionization is greater than that dissipated by the parasitic capacitor, resulting in a rapid rise of I_{DS} . Therefore, the higher delay time causes more holes to accumulate in the substrate, and thus I_{DS} under the higher delay time becomes larger than that under the lower delay time. When enough holes accumulate in the substrate, the substrate potential is so high that the substrate/source p-n⁺ junction is forward-biased; this results in an almost constant substrate potential and I_{DS} tends to be saturated [9]. Therefore, when V_{DS} is sufficiently large, even under different delay times, there are enough holes accumulating in the substrate, resulting in the same substrate potential and the same I_{DS} , as shown in region C in Fig. 2(a) and (b).

At room temperature, the holes can flow to the substrate electrode without accumulation, hence no step-up phenomenon is observed, as shown in Fig. 2(c) and (f). To provide further verification that this phenomenon is related to the substrate potential, we set the substrate electrode to be ungrounded at room temperature, and the step-up effect appears as expected, as shown in Fig. 3(a). Furthermore, the measurement of the substrate current shown in Fig. 3(b) indicates that the impact ionization is more intense at lower V_{GS} . Therefore, the step-up effect is more pronounced at lower V_{GS} .

When V_{DS} is swept in the high-to-low direction, sufficient numbers of holes can accumulate in the substrate instantly because of the high initial V_{DS} . The substrate potential remains constant under higher V_{GS} and decreases monotonously under lower V_{GS} . Therefore, only the splitting behaviors of the curves are observed, as shown in Fig. 2(d) and (e). In addition, at lower temperatures, the reduced ionization rate

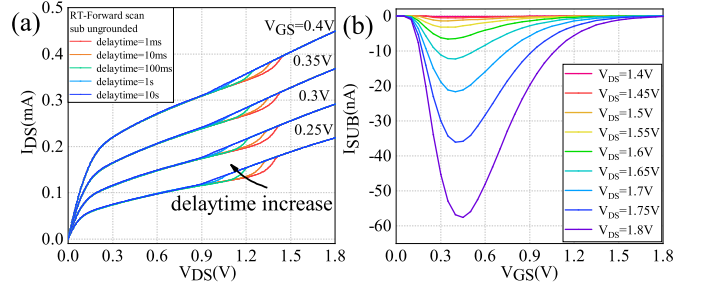


Fig. 3. For the native MOSFETs with $W/L = 10 \mu\text{m}/1 \mu\text{m}$, (a) I-V characteristics when the substrate electrode is ungrounded at room temperature. (b) Substrate current (I_{SUB}) at 4.2 K.

leads to a wider substrate/source depletion width [11]. The capacitance and the time constant of the parasitic capacitor are reduced and thus more holes move to the source through the parasitic capacitance per unit time. Therefore, the splitting behavior becomes more obvious at lower temperatures.

C. Sub-Band Behavior

As shown in Fig. 4(a), a peak transconductance value (G_m -peak) is observed from 40 K to 202 K. This peak value can be attributed to the energy quantization of different sub-bands in the inversion layer [13]. At intermediate temperatures, the carriers occupy the lowest and some higher energy sub-bands with different mobility. V_{GS} changes the distribution of electrons in different sub-bands, thus resulting in a sudden change of the transconductance. However, at lower temperatures, only the lowest energy sub-band is filled and thus no G_m -peak behavior occurs below 40 K. The occupancy of different sub-bands is

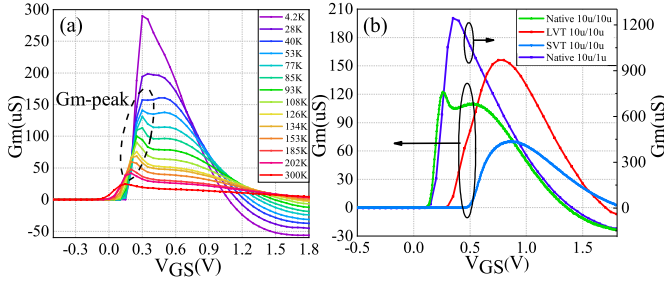


Fig. 4. (a) Transconductance characteristics of native MOSFETs at various temperatures. $V_{DS} = 50$ mV, $W/L = 10 \mu m/10 \mu m$. (b) Comparison of transconductance characteristics of SVT MOSFET ($W/L = 10 \mu m/10 \mu m$), LVT MOSFET ($W/L = 10 \mu m/10 \mu m$), and native MOSFETs ($W/L = 10 \mu m/10 \mu m$ and $W/L = 10 \mu m/1 \mu m$) at 77 K.

related to the longitudinal (i.e., perpendicular to the channel) effective electric field (E_{eff}), which can be calculated as [14]:

$$E_{eff} = (\eta q_{inv} + q_{dep}) / \epsilon_s \quad (1)$$

where $\eta = 0.5$ at room temperature and increases at cryogenic temperature. q_{inv} is the inversion charge per unit area, q_{dep} is the depletion charge per unit area and can be given by:

$$q_{dep} = \sqrt{2q\epsilon_{si}Na\phi_s} \quad (2)$$

where ϕ_s is the surface potential and Na is the substrate doping concentration. To generate the G_m -peak behavior, E_{eff} must be sufficiently low [13], which requires small q_{dep} . The extremely low substrate doping of native MOSFETs can meet this requirement and thus no G_m -peak behavior is observed in the LVT (medium Na) and SVT (standard Na) MOSFETs at 77 K, as shown in Fig. 4(b). Because of the reverse short channel effect (RSCE), the effective Na increases with decreasing channel length. Therefore, G_m -peak behavior is not observed in the native MOSFET with $W/L = 10 \mu m/1 \mu m$, which is consistent with the opinion expressed in [15].

IV. CRYO-MOSFETs MODELING

A. Method: Machine Learning

To obtain more accurate cryogenic MOSFETs (cryo-MOSFETs) model parameters, the parameters are optimized using a machine learning (ML) approach. As shown in Fig. 5(a), the cryo-MOSFETs model was written in both Verilog-A language and C language. The C language code is used to optimize the model parameters in the ML process. The differential evolution (DE) algorithm [16] is used in the optimization process because of its strong global convergence ability and high robustness. The measured data include three characteristics, i.e., the output characteristics and the transfer characteristics in both the linear and the saturation regions. The root-mean-square (RMS) error is introduced to evaluate the fitness of the optimized parameters, which is given by [10]:

$$RMSError = \sqrt{\frac{1}{N} \times \sum_{i=1}^n \left(\frac{I_{measi} - I_{calci}}{I_{measimax}} \right)^2} \times 100\% \quad (3)$$

where N represents the number of data points, I_{meas} and I_{calc} are measured data and calculated data, respectively.

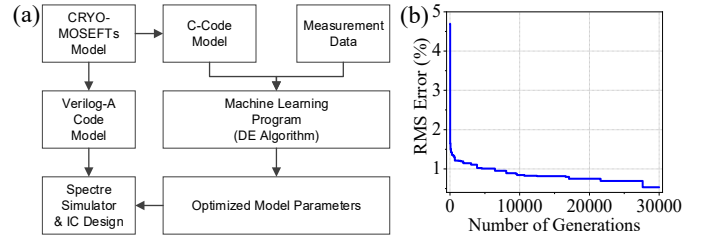


Fig. 5. (a) The flowchart of parameter extraction and modeling process of cryo-MOSFETs via a machine learning approach. (b) RMS error vs the number of generations in a certain optimization process.

$I_{measimax}$ is the maximum measured value. The total RMS error is obtained by averaging the RMS errors of the three characteristics above. As shown in Fig. 5(b), the RMS error decreases monotonically with the optimization process. Finally, the optimized parameters are input into the Verilog-A code model, the results of which can be calculated using commercial simulators and then used in IC design.

B. Modeling

As shown in Fig. 1(b), a serious current drop occurs in the linear region transfer characteristics of native MOSFETs, which is because of the mobility behavior at low temperatures. Even after parameter optimization, the EKV2.6 model cannot describe this phenomenon accurately, as shown in Fig. 6(a). At room temperature, the mobility is mainly determined by the lattice (phonon) scattering and the surface roughness scattering. With increasing V_{GS} , E_{eff} increases and the surface roughness scattering deteriorates, leading to reduced carrier mobility.

At low temperatures, the average phonon number decreases rapidly and the phonon scattering is greatly reduced, even to the point of becoming negligible. The cryogenic mobility is determined by two main scattering processes, i.e., Coulomb scattering of the ionized impurities at lower V_{GS} and surface roughness scattering at higher V_{GS} . The increase of V_{GS} leads to an increase of electron concentration in the inversion layer and the Coulomb mobility is thus elevated. When V_{GS} increases further, the Coulomb scattering becomes less effective than the surface roughness scattering, resulting in a reduction of the mobility. Therefore, the mobility shows a bell-shaped behavior at low temperatures [14], which causes I_{DS} to decrease after an initial increase in the linear region transfer characteristics.

Because the EKV model is compact, concise, and accurate [10], we selected the EKV2.6 model as the basis and then modified the mobility calculation equations to describe the DC characteristics of native MOSFETs accurately over the range from room temperature to cryogenic temperatures. By simplifying the theoretical calculation equations and analyzing the previous measurement results in [17]–[21], we use the following formulas to describe the mobility of the Coulomb scattering (μ_{coul}), the surface roughness scattering (μ_{sr}), and the phonon scattering (μ_{ph}), respectively:

$$\mu_{coul} = \frac{A_0}{(1 + q_{inv}/q_0)^2} \quad (4)$$

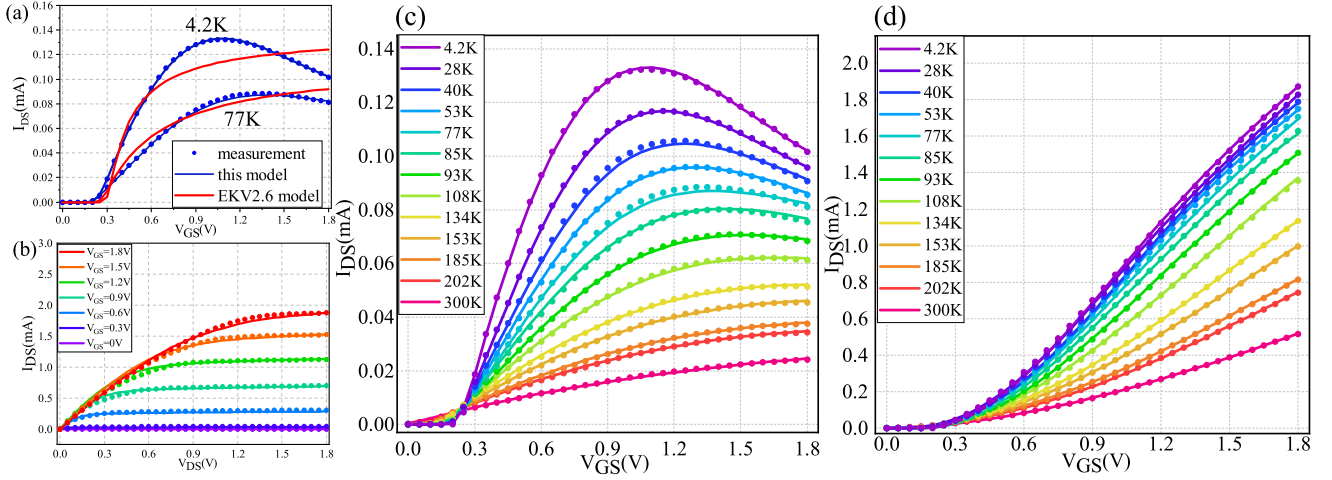


Fig. 6. I-V curves of native MOSFETs with $W/L = 10 \mu\text{m}/10 \mu\text{m}$ measured (symbol) and calculated (solid line) at various temperatures. (a) A comparison of the calculation results between this model and the EKV2.6 model at 77 K and 4.2 K. (b) Measurement and calculation results of the output characteristic at 4.2 K. (c) Measurement and calculation results of the linear region transfer characteristic ($V_{DS} = 50 \text{ mV}$) from 300 K to 4.2 K. (d) Measurement and calculation results of the saturation region transfer characteristic ($V_{DS} = 1.8 \text{ V}$) from 300 K to 4.2 K.

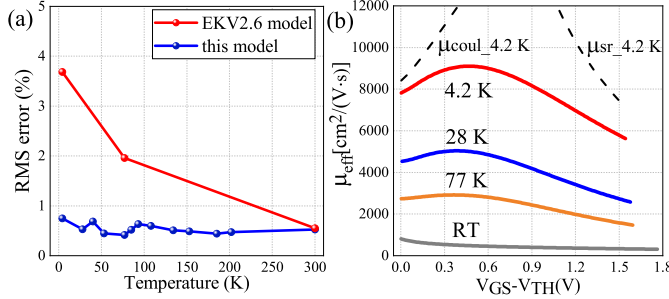


Fig. 7. (a) RMS error of this model and the EKV2.6 model at different temperatures. (b) Calculation results of the effective mobility at RT, 77 K, 28 K and 4.2 K, respectively. The dashed lines are μ_{coul} and μ_{sr} at 4.2 K, respectively.

$$\mu_{sr} = \frac{1}{A_1 \times E_{eff}^2} \quad (5)$$

$$\mu_{ph} = A_2 \times (q_{inv} + q_{dep})^{-1/3} \quad (6)$$

where q_{inv} , q_{dep} and E_{eff} are the same physical quantities as (1), and A_0 , A_1 , A_2 are model parameters. q_0 is a parameter related to ionized impurities. q_{inv} and q_{dep} are calculated by the default equations of EKV2.6 model. According to Mathiessen's rule, the effective mobility (μ_{eff}) is given by:

$$\frac{1}{\mu_{eff}} = \frac{1}{\mu_{coul}} + \frac{1}{\mu_{sr}} + \frac{1}{\mu_{ph}} \quad (7)$$

Eq. (7) is associated with EKV2.6 model by $\beta = \mu_{eff} \times C_{OX} \times W/L \times 10^{-4}$. β is a default variable related to mobility in EKV2.6 model [5] and the unit of μ_{eff} is $\text{cm}^2/(\text{V}\cdot\text{s})$.

The calculation results are presented in Fig. 6. As expected, the results show the intersection behavior in the output characteristics at 4.2 K, as shown in Fig. 6(b). Fig. 6(c) and (d) show the linear region and the saturation region transfer characteristics from 300 K to 4.2 K, respectively. The RMS error of the calculation results is less than 0.75% at each

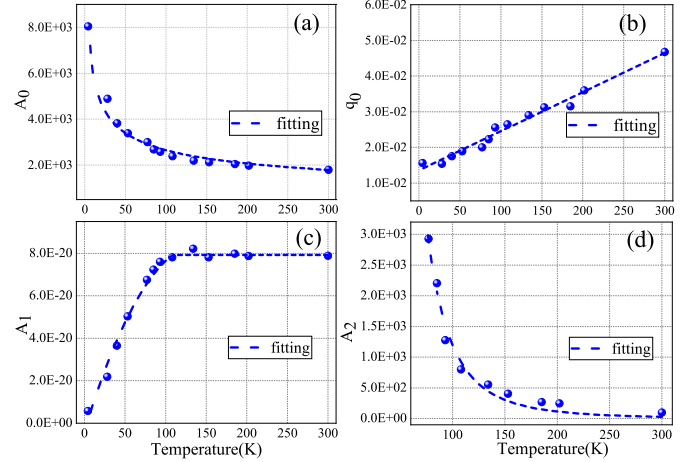


Fig. 8. The mobility-related parameters vs temperature. (a) A_0 . (b) q_0 . (c) A_1 . (d) A_2 . The points are the mobility-related parameters at specific temperatures extracted via the machine learning approach and the dotted lines are fitting lines.

temperature, as shown in Fig. 7(a), and is much smaller than the corresponding results of the original EKV2.6 model. It is concluded that the proposed model is applicable from room temperature to liquid helium temperature.

The variation of the parameters with temperature is also worthy of discussion. Because its influence is negligible, we did not consider the phonon scattering below 77 K. Fig. 8(a) and (b) show the variations of Coulomb scattering related parameters (i.e., A_0 , q_0). With decreasing temperature, the average velocity of the carriers increases, which means that carriers can pass through the Coulomb potential field of the ionized impurity atoms in a shorter time. Therefore, the carrier deflection angle under Coulomb scattering becomes smaller and the scattering probability is reduced, which results in a monotonic increase of A_0 with decreasing temperature. Additionally, the ionization rate decreases at low temperatures, and thus only a few impurities can be ionized to form Coulomb

centers, resulting in the decrease of q_0 . The combination of the two mechanisms above leads to a higher μ_{coul} value at lower temperatures. The variation of A_0 and q_0 with temperature can be fitted as follows, respectively: $A_0 = 1.4 \times 10^4 \times T^{-0.357}$, $q_0 = 1.1 \times 10^{-4}T + 0.014$.

The variation of the surface roughness scattering coefficient (A_1) with temperature is shown in Fig. 8(c). A_1 remains almost constant above 110 K but decreases with decreasing temperature below 110 K, which is likely to be caused by the degeneracy effect. At cryogenic temperatures, the carriers become strongly degenerate [22], resulting in a reduction of the surface roughness scattering under high electric fields [17]. The cryogenic degeneracy effect is negligible above 110 K, so A_1 is almost unchanged in that range. The variation of A_1 with temperature can be fitted as follows: $A_1 = -4.4 \times 10^{-24}T^2 + 1.2 \times 10^{-21}T - 3.5 \times 10^{-21}$ ($T < 110$ K) and $A_1 \approx 7.93 \times 10^{-20}$ ($T > 110$ K). Although A_1 is almost unchanged above 110 K, due to $q_{inv} \approx Cox(V_{GS} - V_{TH})$, higher temperature leads to a smaller V_{TH} , i.e., q_{inv} and E_{eff} increase, resulting in the decrease of μ_{sr} with increasing temperature.

The variation of the phonon scattering coefficient is shown in Fig. 8(d). A_2 increases significantly with decreasing temperature and can be fitted as $A_2 = 6.6 \times 10^9 T^{-3.4}$. Furthermore, the calculation results of μ_{eff} at specific temperatures are shown in Fig. 7(b). The variation trend of μ_{eff} shows a bell-shaped behavior at low temperatures, which is consistent with the theoretical predictions.

V. CONCLUSION

Native MOSFETs can be used in high-speed or low power consumption circuits. In this paper, commercial 0.18 μm native MOSFETs are characterized in the temperature range from 300 K to 4.2 K. With decreasing temperature, V_{TH} increases up to ~ 0.25 V ($W/L = 10 \mu\text{m}/10 \mu\text{m}$) and the improved $SS \approx 14.30$ mV/dec @ 4.2 K. The I_{off} , the GIDL induced leakage, and the ON/OFF ratio are ameliorated obviously, but the DIBL effect shows deterioration. In addition, the step-up effect and the G_m -peak effect are observed and discussed. By using Coulomb scattering, surface roughness scattering, and phonon scattering to calculate the carrier mobility, a compact model of large size native MOSFETs suitable for the range of 300 K to 4.2 K is proposed. This model is able to fit the DC characteristics very well, particularly the current drop behavior in the linear region. In addition, the mobility-related parameters are extracted via a machine learning approach and the temperature dependences of the scattering mechanisms are analyzed. This work contributes to the research of cryo-MOSFETs physics and also lays a foundation for cryo-CMOS circuit design.

REFERENCES

- [1] E. Charbon, F. Sebastiano, A. Vladimirescu, H. Homulle, S. Visser, L. Song, and R. M. Incandela, "Cryo-CMOS for quantum computing," in *IEDM Tech. Dig.*, Dec. 2016, pp. 13–15, doi: 10.1109/IEDM.2016.7838410.
- [2] B. Patra, R. M. Incandela, J. P. G. van Dijk, H. A. R. Homulle, L. Song, M. Shahmohammadi, R. B. Staszewski, A. Vladimirescu, M. Babaie, F. Sebastiano, and E. Charbon, "Cryo-CMOS circuits and systems for quantum computing applications," *IEEE J. Solid-State Circuits*, vol. 53, no. 1, pp. 309–321, Jan 2018, doi: 10.1109/JSSC.2017.2737549.
- [3] T.-Y. Yang, A. Ruffino, J. Michniewicz, Y. Peng, E. Charbon and M. F. Gonzalez-Zalba, "Quantum Transport in 40-nm MOSFETs at Deep-Cryogenic Temperatures," *IEEE Electron Device Lett.*, vol. 41, no. 7, pp. 981–984, 2020, doi: 10.1109/LED.2020.2995645.
- [4] Y. Cheng, M. Chan, K. Hui, M. Jeng, Z. Liu, J. Huang, K. Chen, J. Chen, R. Tu, P.K. Ko and Chenming Hu, "BSIM 3v3 manual (final version)," Dept. Elect. Eng. Comput. Sci., Univ. California, Berkeley, CA, USA, Rep. UCB/ERL M97/2, 1997.
- [5] M. Bucher, C. Lallemand, C. Enz, F. Théodoloz, and F. Krummenacher, *The EPFL-EKV MOSFET Model Equations for Simulation Model Version 2.6*, Dept. Electron. Lab, Swiss Federal Inst. Technol. (EPFL), Lausanne, Switzerland, Jun. 1997.
- [6] M. Shin, M. Shi, M. Mouis, A. Cros, E. Josse, G. T. Kim and G. Ghibaudo, "Low temperature characterization of 14nm FDSOI CMOS devices," in *Proc. 11th Int. Workshop Low Temp. Electron. (WOLTE)*, pp. 29–32, 2014, doi: 10.1109/WOLTE.2014.6881018.
- [7] C. Luo, Z. Li, T. Lu, J. Xu, and G. Guo, "MOSFET characterization and modeling at cryogenic temperatures," *Cryogenics*, vol. 98, pp. 12–17, 2019, doi: 10.1016/j.cryogenics.2018.12.009.
- [8] A. Beckers, F. Jazaeri and C. Enz, "Characterization and Modeling of 28-nm Bulk CMOS Technology Down to 4.2 K," *IEEE J. Electron Devices Soc.*, vol. 6, pp. 1007–1018, 2018, doi: 10.1109/JEDS.2018.2817458.
- [9] R. M. Incandela, L. Song, H. Homulle, E. Charbon, A. Vladimirescu and F. Sebastiano, "Characterization and Compact Modeling of Nanometer CMOS Transistors at Deep-Cryogenic Temperatures," *IEEE J. Electron Devices Soc.*, vol. 6, pp. 996–1006, 2018, doi: 10.1109/JEDS.2018.2821763.
- [10] T.-T. Lu, Z. Li, C. Luo, J. Xu, W. Kong and G. Guo, "Characterization and Modeling of 0.18 μm Bulk CMOS Technology at Sub-Kelvin Temperature," *IEEE J. Electron Devices Soc.*, vol. 8, pp. 897–904, 2020, doi: 10.1109/JEDS.2020.3015265.
- [11] Y. Liu, L. Lang, Y. Chang, Y. Shan, X. Chen and Y. Dong, "Cryogenic Characteristics of Multinanoscale Field-Effect Transistors," *IEEE Trans. Electron Devices*, vol. 68, no. 2, pp. 456–463, 2021, doi: 10.1109/TED.2020.3041438.
- [12] F. Balestra, L. Audaire, and C. Lucas, "Influence of substrate freeze-out on the characteristics of MOS transistors at very low temperatures," *Solid-State Electron.*, vol. 30, no. 3, pp. 321–327, 1987, doi:10.1016/0038-1101(87)90190-0.
- [13] P. Marti, M. Cavelier, R. Fascio, G. Ghibaudo and M. Bucher, "EKV3 compact modeling of MOS transistors from a 0.18 μm CMOS technology for mixed analog–digital circuit design at low temperature," *Cryogenics*, vol. 49, no. 11, pp. 595–598, 2009, doi: 10.1016/j.cryogenics.2008.12.005.
- [14] A. Hairapetian, D. Gitlin and C. R. Viswanathan, "Low-temperature mobility measurements on CMOS devices," *IEEE Trans. Electron Devices*, vol. 36, no. 8, pp. 1448–1455, 2021, doi: 10.1109/16.30958.
- [15] P. Martin, A.S. Royet, F. Guellec, G. Ghibaudo, "MOSFET modeling for design of ultra-high performance infrared CMOS imagers working at cryogenic temperatures: Case of an analog/digital 0.18 μm CMOS process," *Solid-State Electron.*, vol. 62, no. 1, pp. 115–122, 2011, doi:10.1016/j.sse.2011.01.004.
- [16] Price, Kenneth V., "Differential Evolution," *Handbook of Optimization: From Classical to Modern Approach*, pp. 187–214, 2013, doi: 10.1007/978-3-642-30504-7_8.
- [17] S. Yamakawa, H. Ueno, K. Taniguchi, C. Hamaguchi, K. Miyatsuji, K. Masaki, and U. Ravaioli, "Study of interface roughness dependence of electron mobility in Si inversion layers using the Monte Carlo method," *J. Appl. Phys.*, vol. 79, no. 2, pp. 911–916, 1996, doi: 10.1063/1.360871.
- [18] S. Kawaji, "The Two-Dimensional Lattice Scattering Mobility in a Semiconductor Inversion Layer," *J. Phys. Soc. Jpn.*, vol. 27, no. 4, pp. 906–908, 1969, doi: 10.1143/JPSJ.27.906.
- [19] Y. C. Cheng, E. A. Sullivan, "Effect of Coulomb scattering on silicon surface mobility," *J. Appl. Phys.*, vol. 45, no. 1, pp. 187–192, 1974, doi: 10.1063/1.1662957.
- [20] O. Katz, A. Horn, G. Bahir and J. Salzman, "Electron mobility in an AlGaIn/GaN two-dimensional electron gas. I. Carrier concentration dependent mobility," *IEEE Trans. Electron Devices*, vol. 50, no. 10, pp. 2002–2008, 2003, doi: 10.1109/TED.2003.816103.
- [21] G. S. Gildenblat, C.-L. HUANG, "Engineering model of inversion channel mobility for 60–300 K temperature range," *Electron. Lett.*, vol. 25, no. 10, pp. 634–636, 1989, doi: 10.1049/el:19890430.
- [22] M. Kantner, T. Koprucki, "Numerical simulation of carrier transport in semiconductor devices at cryogenic temperatures," *Opt. Quant. Electron.*, vol. 48, no. 543, 2016, doi: 10.1007/s11082-016-0817-2.